JACS
JOURNAL OF THE AMERICAN CHEMICAL SOCIETY

Communication

Photocatalytic CO Reduction Using a Robust Multifunctional Iridium Complex towards the Selective Formation of Formic Acid

Kenji Kamada, Jieun Jung, Wakabayashi Taku, Keita Sekizawa, Shunsuke Sato, Takeshi Morikawa, Shunichi Fukuzumi, and Susumu Saito

J. Am. Chem. Soc., **Just Accepted Manuscript** • DOI: 10.1021/jacs.0c03097 • Publication Date (Web): 26 May 2020

is published by the American Chemical Society. 1155 Sixteenth Street N.W., Washington, DC 20036

Photocatalytic CO_2 Reduction Using a Robust Multifunctional Iridium Complex towards the Selective Formation of Formic Acid

Kenji Kamada,[†] Jieun Jung*,[†] Taku Wakabayashi,[†] Keita Sekizawa,[‡] Shunsuke Sato,[‡] Takeshi Morikawa,[‡] Shunichi Fukuzumi,[§] and Susumu Saito*,[†,||]

[†]Department of Chemistry, Graduate School of Science, Nagoya University, Chikusa, Nagoya 464-8602, Japan

[‡]Toyota Central R&D Labs., Inc., 41-1 Yokomichi, Nagakute 480-1192, Japan

[§]Faculty of Science and Engineering, Meijo University, Nagoya 468-8502, Japan

[||]Research Center for Materials Science (RCMS), Nagoya University, Chikusa, Nagoya 464-8602, Japan.

Supporting Information Placeholder

ABSTRACT: A highly efficient tetradentate PNNP-type Ir photocatalyst, Mes-IrPCY2, was developed for the reduction of carbon dioxide (CO_2). The photocatalyst furnished formic acid (HCO_2H) with 87% selectivity together with carbon monoxide (CO) to achieve a turnover number of 2560, which is the highest among CO_2-reduction photocatalysts without an additional photosensitizer. Mes-IrPCY2 exhibited outstanding photocatalytic CO_2-reduction activity in the presence of the sacrificial electron source 1,3-dimethyl-2-phenyl-2,3-dihydro-1*H*-benzo[*d*]-imidazole (BIH) in CO_2-saturated *N,N*-dimethylacetamide (DMA) under irradiation with visible light. The quantum yield was determined to be 49% for the generation of HCO_2H and CO. Electron paramagnetic resonance (EPR) and UV-vis spectroscopy studies of Mes-IrPCY2 with a sacrificial electron donor revealed that the one-electron reduced species is the key intermediate for the selective formation of HCO_2H.

The development of systems for the synthesis of value-added organic substances from carbon dioxide (CO_2) has become increasingly popular as a key strategy to solve the problems of global warming and fossil fuel shortages.[1,2] In particular, formic acid (HCO_2H), a platform chemical that can be obtained from the reduction of CO_2 and used in applications such as direct formic acid fuel cells (DFAFCs),[3] could represent a valuable energy-storage source. Photocatalytic CO_2 reduction has attracted extensive interest, since the photocatalytic conversion of CO_2 to energy-enriched compounds could potentially be achieved under relatively mild conditions.[4] However, because the homogeneous photochemical reduction of CO_2 is an inherently difficult-to-control multi-electron reduction, two-component systems involving a transition-metal catalyst, photosensitizer, and sacrificial reductant or supramolecular systems have typically been used to achieve the photocatalytic reduction of CO_2.[5,6]

Scheme 1. Photocatalytic Reduction of CO_2 with an Ir Complex under Photoirradiation ($\lambda \geq 400$ nm)

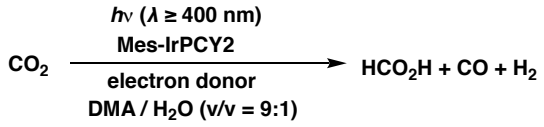

Several examples of single-active-site photocatalysts that function as both the photosensitizer and catalyst for CO_2 reduction based on Re,[7] Os,[8] Ir,[9] Ru,[10] and other metals[11] have been reported. The development of self-photosensitized metal complexes is advantageous in terms of lowering the activation energy of the catalytic reaction and controlling its selectivity; thus, extensive efforts have been devoted to designing new molecular photocatalysts by changing the metal center and/or ligands. However, the development of robust homogeneous photocatalysts has remained challenging as most exhibit low turnover numbers (TON), and photocatalysts that can produce HCO_2H selectively by CO_2 photoreduction are very rare.[7d,9e]

Herein, we introduce Mes-IrPCY2 (**1**) as a structurally robust, tetradentate PNNP-type Ir complex (Figure 1, inset) for the photocatalytic reduction of CO_2 to HCO_2H. This CO_2-reduction photocatalyst produces mainly HCO_2H with high activity and selectivity without requiring an additional photosensitizer. From a molecular engineering perspective, the key aspects for the design of this catalyst are: i) the introduction of a bulky PNNP-ligand, which has been

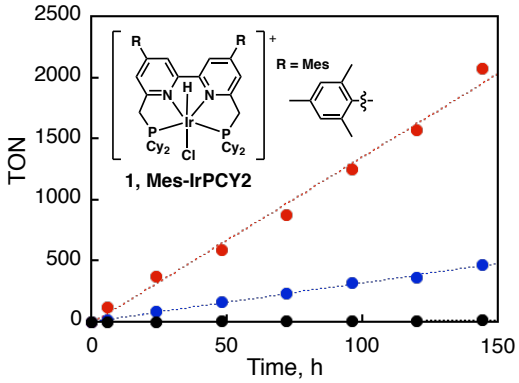

Figure 1. Time course plots of the products [HCO_2H (red), CO (blue), and H_2 (black)] obtained during the photocatalytic reduction of CO_2 with a catalytic amount of Mes-IrPCY2 (20 μM) and BIH (0.2 M) in a CO_2-saturated mixture of DMA:H_2O (9:1, v/v) under photoirradiation ($\lambda \geq 400$ nm) at 298 K. The inset shows the chemical structure of Mes-IrPCY2 (**1**).

shown to prevent catalyst deterioration and promote efficient hydrogenation,[12] and ii) the incorporation of bipyridyl CH_2P groups, which could potentially act as proton donors. The bulky PNNP ligands were expected to control the stereochemistry at the metal atom and effectively reduce CO_2 under photoirradiation conditions.[13] Given that metal complexes that bear bipyridyl CH_2P groups can act as hydrogenation catalysts via an outer-sphere mechanism, we anticipated that **1** would successfully produce HCO_2H by CO_2 photoreduction via outer-sphere catalysis, accompanied by inner-sphere catalysis to produce CO, as many previous examples have suggested.[7, 8b, 9c, 10a, 11] In other words, **1** is potentially a multifunctional photocatalyst that could function as both a photosensitizer and a catalyst that could reduce CO_2 to HCO_2H and CO via outer-sphere and inner-sphere catalysis, respectively.

The photocatalytic reduction of CO_2 was examined by photoirradiation ($\lambda \geq 400$ nm) of a mixed dimethylacetamide (DMA) and H_2O (v/v = 9:1) solution containing **1** and the sacrificial electron donor 1,3-dimethyl-2-phenyl-2,3-dihydro-1*H*-benzo[*d*]imidazole (BIH) under 1 atm of CO_2 (Scheme 1). Efficient CO_2 reduction occurred, with TONs of 2080(50), 470(10), and 15(1) for HCO_2H, CO, and H_2, respectively. Plots of the time course of the formation of each product by **1** are shown in Figure 1; the amount of HCO_2H and CO produced continually increased with irradiation time for over 1 week, indicating that **1** exhibits sufficient robustness in this photocatalytic reaction.[14] A mercury test also revealed that photocatalytic reduction of CO_2 occurred by homogeneous catalyst (Table S1; entry 1 and 2), exhibiting no significant difference in the amount of product in the presence of Hg (0.17 M). Negligible amounts of the products were produced in control experiments in the absence of **1** or CO_2 (Figure S1). A labeling experiment was performed with ^{13}C-labeled CO_2 ($^{13}CO_2$) in a $^{13}CO_2$-saturated mixture of DMF-d_7/ H_2O (v/v = 9:1) to determine the carbon source of the products. The $^{13}CO_2$-labeling experiments indicated that the CO_2 gas was the source of the carbon atoms in the generated HCO_2H (Figure S2). The quantum yield (QY = 49% at λ = 400 nm) was determined using a ferroxalate actinometer,[15] and the selectivity towards HCO_2H was 87% (*cf.* experimental section and Figure S3). When triethanolamine (TEOA), which is commonly used as an electron donor in this field, was used instead of BIH, however, the reactivity decreased significantly and the selectivity for HCO_2H was lost (Figure S4 in SI).

In order to study the photophysical properties of **1**, sub-nanosecond laser-induced transient absorption (picoTAS) measurements[16] were performed on **1**. Laser excitation of a deaerated DMA solution of **1** resulted in the formation of a long-lived excited state with an absorption band at λ_{max} = 500 nm (Figure 2a). This new absorption was assigned to the triplet (T_1) excited state. Intersystem crossing processes from the singlet (S_1) excited state to the T_1 state are known to be extremely rapid due to strong spin-orbit coupling.[17] From the decay time profile of the absorbance at 500 nm, the lifetime of the T_1 state of **1** was determined to be τ = 173(13) ns at 298 K (Figure 2a, inset).

When ferrocene was added to a deaerated DMA solution of **1** as an electron donor, the decay of the absorbance at 500 nm due to the T_1 excited state of **1** was accelerated, and the decay rate constant increased linearly with increasing concentration of ferrocene (Figure 2b). These results indicate that electron transfer occurred from ferrocene to the T_1 excited state of **1**. The rate constant of electron transfer from ferrocene to the T_1 excited state of **1** was determined to be [$(3.2 \pm 0.3) \times 10^9$ M^{-1} s^{-1} at 298 K] from the slope of the linear plot of k_{obs} as a function of the ferrocene concentration (Figure 2b). The rate constants of electron transfer (k_{et}) from various ferrocene

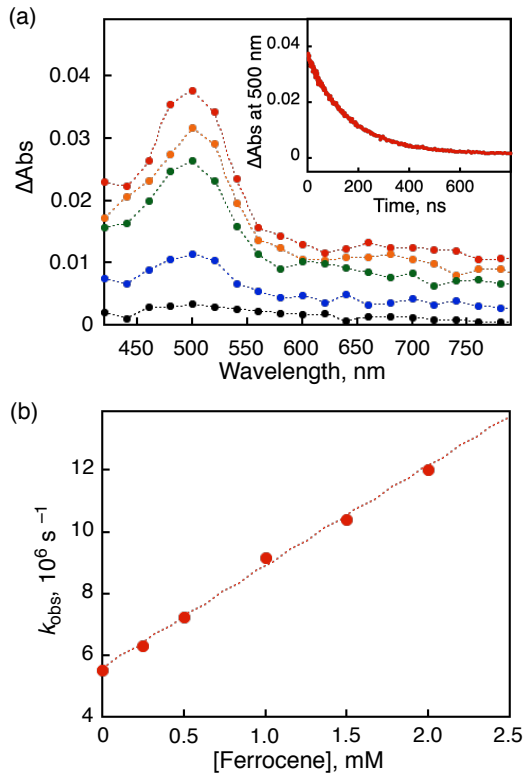

Figure 2. (a) Transient absorption spectral changes (red: 2 ns; orange: 20 ns; green: 50 ns; blue: 200 ns; black: 500 ns) after sub-nanosecond laser excitation at 355 nm in a deaerated DMA solution of **1** (1.0 mM) at 298 K. Inset shows the decay time profile of the absorbance at 500 nm due to the decay of the excited state of **1**. (b) Plot of k_{obs} vs the concentration of ferrocene in a DMA solution at 298 K.

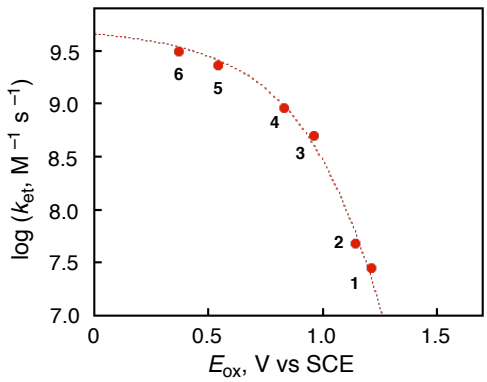

Figure 3. Plot of log k_{et} of photoinduced electron transfer from methoxybenzene derivatives and ferrocene derivatives [1: 1,4-dimethoxybenzene; 2: 1,2,3,4-tetramethoxybenzene; 3: 1,2,4-trimethoxybenzene; 4: triphenylamine; 5: bromoferrocene; 6: ferrocene] to the excited state of **1** in DMF at 298 K.

and methoxybenzene derivatives to the T_1 excited state of **1** were determined in the same manner, and the k_{et} values are listed in Table S2 (Figures S5–S9). The plot of log k_{et} as a function of the one-electron oxidation potentials of the electron donors (E_{ox}) (Figure 3) exhibits the expected behavior, i.e., the log k_{et} value increases with decreasing E_{ox} to reach a diffusion-limited maximum, as expressed by the Marcus equation of intermolecular electron transfer (eq 1):

$$1/k_{et} = 1/k_{diff} + 1/(Z\exp[(-\lambda/4)(1 + \Delta G_{et}/\lambda)^2/(k_B T)]) \quad (1)$$

Scheme 2. Proposed Mechanism of the Photocatalytic Reduction of CO_2 Using Mes-IrPCY2 (1)

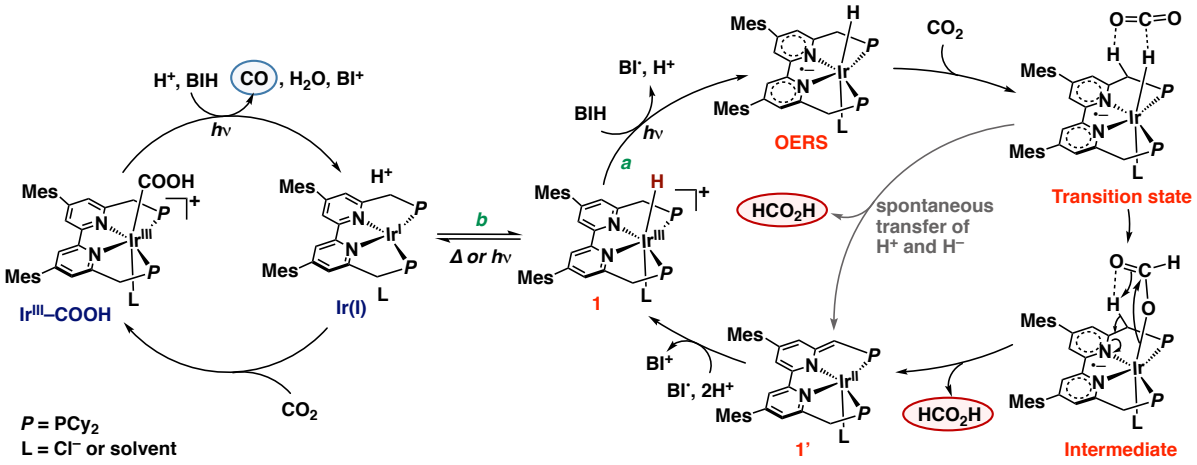

where λ is the reorganization energy of electron transfer, k_{diff} is the diffusion rate constant, Z is the collision frequency, which is taken as 10^{11} M^{-1} s^{-1}, k_B is the Boltzmann constant and T is the absolute temperature.[18,19]

The Gibbs energy change associated with the electron transfer, ΔG_{et}, is given by eq 2:

$$\Delta G_{et} = e(E_{ox} - E_{red}) \quad (2)$$

where e is the elementary charge and E_{red} the one-electron reduction potential of the electron acceptor. The best fit in Figure 3 gives an E_{red} value of 1.32(1) V for [**1**]*, along with a λ of 0.90(4) eV, and a k_{diff} of 7.0×10^9 M^{-1} s^{-1}.

The electron-transfer rate constant (k_2) of BIH was determined to be $(2.5 \pm 0.1) \times 10^9$ M^{-1} s^{-1} (Figure S10), which is significantly larger than that of TEOA ($(1.2 \pm 0.1) \times 10^8$ M^{-1} s^{-1}; Figure S11), being consistent with the more negative one-electron oxidation potential of BIH (E_{ox} = 0.21 V vs SCE in DMA) compared to that of TEOA (E_{ox} = 0.68 V vs SCE in DMA) (Figure S12).[20]

Formation of the one-electron reduced species (OERS) in the photo-driven reduction of **1** (Scheme 2, reaction pathway *a*) was observed via the change in the UV-vis spectrum. Upon photoirradiation, a UV-vis spectral change was observed from **1** to a new absorption band at 569 nm, which showed that the rate constant of the OERS formation (k_{obs}) increased with increasing concentration of BIH (Figure S13). The formation of the OERS was also confirmed

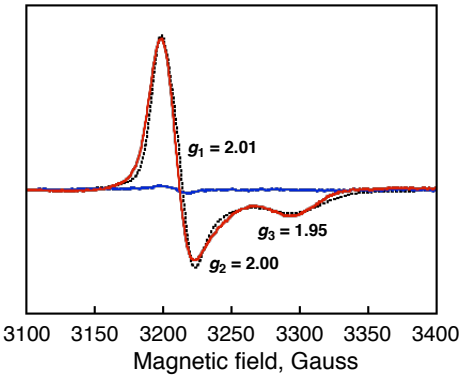

Figure 4. X-band EPR spectrum of **1** obtained after 0 min (blue line) and 10 min (red line for experimental and black for simulated) of photoirradiation ($\lambda \geq 400$ nm) in an Ar-saturated mixture of DMA/H_2O (v/v = 9:1) containing **1** (1.0 mM) and BIH (0.1 M) at 173 K.

by electron paramagnetic resonance (EPR) measurements of a mixed DMA/H_2O (v/v = 9:1) solution containing **1** and BIH under photoirradiation at 173 K; a new EPR signal corresponding to the OERS (g_1 = 2.01; g_2 =2.00; g_3 =1.95 and line widths of ΔB_1 = 12 G, ΔB_2 = 13 G, and ΔB_3 = 37 G) is shown in Figure 4.[21,22] The electrochemical characterization of **1** indicates that after the one-electron reduction of **1** at –1.22 V vs SCE assignable to a reduction potential for the ligand of **1** [P(bpy)P/P(bpy$^{\bullet-}$)P],[23] the OERS reacted with CO_2 to give catalytic current growth under CO_2 (Figure S14).

When BIH was replaced with TEOA, deprotonation of Ir^{III}-H to give an Ir^{I} species (Scheme 2, reaction pathway *b*) rather than the OERS was predominantly observed (Figure S15). The rate constant for the deprotonation of **1** is independent of the concentration of TEOA (Figure S15c). ^{1}H NMR spectrum of Ir(III)–H showed disappearance of the ^{1}H NMR triplet signal of the hydride by photoirradiation, indicating deprotonation of Ir(III)–H occurred to form Ir(I) without BIH nor TEOA. Additionally, it was observed that the hydrogen atoms of CH_2P group are all replaced with deuterium atoms, indicating that the methylene hydrogen atoms are acidic enough to be deprotonated under photoirradiation in DMA-d_9/D_2O (9:1, v/v) (Figure S16). The deprotonation of the excited state of **1** is also consistent with a previous report[24] that revealed that the metal-to-ligand charge-transfer due to the excitation reduces the basicity of the Ir center, facilitating the release of a proton from the Ir complex (Figure S17; DFT calculations).

Based on the experimental results described above, a mechanism for the photocatalytic reduction of CO_2 by **1** in the presence of an electron donor is proposed in Scheme 2. In reaction pathway *a*, photo-excited Ir^{III}–H (**1**) is reduced to OERS by fast electron transfer from BIH, followed by the insertion of CO_2 into the Ir-H bond to give the corresponding transition state and intermediate.[25] A nucleophilic attack on CO_2 leads to an H-bonded formate intermediate, followed by dissociation of HCO_2H and regeneration of **1**. Spontaneous proton and hydride transfer cannot be comprehensively ruled out at this point.[26] In reaction pathway *b*, deprotonation of **1** leads to the corresponding Ir^{I} species, which reacts with CO_2 to give the Ir^{III}-COOH species, followed by release of CO and regeneration of Ir^{I}. In the proposed mechanism, the rapid one-electron transfer process for the formation of OERS results in the release of HCO_2H via outer-sphere catalysis, whereas the deprotonation of **1** leads to the evolution of CO via inner-sphere catalysis.[27,28]

In conclusion, a new multifunctional PNNP-type Ir complex photocatalyst (**1**) has been developed that functions as both a photosensitizer and a catalyst to reduce CO_2 to HCO_2H via outer-sphere catalysis and to CO via inner-sphere catalysis. The total TON for the photocatalytic reduction of CO_2 is 2560, with 87% HCO_2H selectivity in the presence of BIH as an electron donor. We have clarified the reaction pathways using experimental data, which indicates that the initial step of the catalytic cycle is critical for the selective reduction of CO_2. The reactivity and robustness of the catalyst are significantly enhanced by the introduction of a PNNP-type ligand. The present study has thus provided new insights into the development of efficient catalysts for CO_2 reduction reactions.

ASSOCIATED CONTENT

Supporting Information.

Experimental details, Scheme S1, Table S1 – S2 and Figures S1 – S27. This material is available free of charge via the Internet at http://pubs.acs.org.

AUTHOR INFORMATION

Corresponding Author

*jieun@chem.nagoya-u.ac.jp

*saito.susumu@f.mbox.nagoya-u.ac.jp

ORCID

Kenji Kamada: 0000-0002-2532-5448

Jieun Jung: 0000-0002-5310-8643

Taku Wakabayashi: 0000-0002-2083-3590

Keita Sekizawa: 0000-0003-2660-0410

Shunsuke Sato: 0000-0001-8178-7367

Takeshi Morikawa: 0000-0002-4985-0925

Shunichi Fukuzumi: 0000-0002-3559-4107

Susumu Saito: 0000-0003-0749-2020

Notes

The authors declare no competing financial interest.

ACKNOWLEDGMENT

We thank Dr. Kin-ichi Oyama (Nagoya University) for elemental analysis. This work was supported by Grant-in-Aid for Early-Career Scientists (no. 18K14241 to J. J.), Scientific Research (B) (no. 19H02713 to S.S.), and Grant-in-Aid (no. 16H02268 to S.F.) from the Japanese Society for the Promotion of Science (JSPS) and Asahi Glass Foundation (Step-up-grant to S. S.) and a Grant-in-aid for Scientific Research on Innovative Areas (no. 18H04247 to S.S.) from the Japanese Ministry of Education, Culture, Sports, Science and Technology (MEXT), as well as from the Ministry of the Environment Government of Japan.

REFERENCES

(1) (a) Luo, Y.-H.; Dong, L.-Z.; Liu, J.; Li, S.-L.; Lan, Y.-Q. From Molecular Metal Complex to Metal-Organic Framework: The CO_2 Reduction Photocatalysts with Clear and Tunable Structure. *Coord. Chem. Rev.* **2019**, *390*, 86–126. (b) Francke, R.; Schille, B; Roemelt. M. Homogeneously Catalyzed Electroreduction of Carbon Dioxide–Methods, Mechanisms, and Catalysts. *Chem. Rev.* **2018**, *118*, 4631–4701.

(2) (a) Sahara, G.; Ishitani, O. Efficient Photocatalysts for CO_2 Reduction. *Inorg. Chem.* **2015**, *54*, 5096–5104. (b) Fukuzumi, S.; Lee, Y.-M.; Ahn, H. S.; Nam, W. Mechanisms of Catalytic Reduction of CO_2 with Heme and Nonheme Metal Complexes. *Chem. Sci.* **2018**, *9*, 6017–6034.

(3) (a) Rumayor, M.; Dominguez-Ramos, A.; Irabien, A. Formic Acid Manufacture: Carbon Dioxide Utilization Alternatives. *Appl. Sci.* **2018**, *8*, 914/1–914/12. (b) Huang, J.; Wang, L. Bifunctional Wood for Electrocatalytic CO_2 Reduction to Formate and Electroanalytical Detection of Myricetin and Cadmium (II). *Electrochim. Acta* **2019**, *319*, 569–576.

(4) (a) Chen, Z.; Zhang, H.; Guo, P.; Zhang, J.; Tira, G.; Kim, Y. J.; Wu, Y. A.; Liu, Y.; Wen, J.; Rajh, T.; Niklas, J.; Poluektov, O. G.; Laible, P. D.; Rozhkova, E. A. Semi-artificial Photosynthetic CO_2 Reduction through Purple Membrane Re-engineering with Semiconductor. *J. Am. Chem. Soc.* **2019**, *141*, 11811–11815. (b) Zhang, S.; Xia, Z.; Zou, Y.; Cao, F.; Liu, Y.; Ma, Y.; Qu, Y. Interfacial Frustrated Lewis Pairs of CeO_2 Activate CO_2 for Selective Tandem Transformation of Olefins and CO_2 into Cyclic Carbonates. *J. Am. Chem. Soc.* **2019**, *141*, 11353–11357. (c) Kuriki, R.; Ichibha, T.; Hongo, K.; Lu, D.; Maezono, R.; Kageyama, H.; Ishitani, O.; Oka, K.; Maeda, K. A Stable, Narrow-Gap Oxyfluoride Photocatalyst for Visible-Light Hydrogen Evolution and Carbon Dioxide Reduction. *J. Am. Chem. Soc.* **2018**, *140*, 6648–6655.

(5) (a) Shirley, H.; Su, X.; Sanjanwala, H.; Talukdar, K.; Jurss, J. W.; Delcamp, J. H. Durable Solar-Powered Systems with Ni-Catalysts for Conversion of CO_2 or CO to CH_4. *J. Am. Chem. Soc.* **2019**, *141*, 6617–6622. (b) Fogeron, T.; Retailleau, P.; Chamoreau, L.-M.; Li, Y.; Fontecave, M. Pyranopterin Related Dithiolene Molybdenum Complexes as Homogeneous Catalysts for CO_2 Photoreduction. *Angew. Chem., Int. Ed.* **2018**, *57*, 17033–17037. (c) Rohacova, J.; Ishitani, O. Rhenium(I) Trinuclear Rings as Highly Efficient Redox Photosensitizers for Photocatalytic CO_2 Reduction. *Chem. Sci.* **2016**, *7*, 6728–6739. (d) Ouyang, T.; Huang, H.-H.; Wang, J.-W.; Zhong, D.-C.; Lu, T.-B. A Dinuclear Cobalt Cryptate as a Homogeneous Photocatalyst for Highly Selective and Efficient Visible-Light Driven CO_2 Reduction to CO in CH_3CN/H_2O Solution. *Angew. Chem., Int. Ed.* **2017**, *56*, 738–743. (e) Burks, D. B.; Davis, S.; Lamb, R. W.; Liu, X.; Rodrigues, R. R.; Liyanage, N. P.; Sun, Y.; Webster, C. E.; Delcamp, J. H.; Papish, E. T. Nickel(II) Pincer Complexes Demonstrate that the Remote Substituent Controls Catalytic Carbon Dioxide Reduction. *Chem. Commun.* **2018**, *54*, 3819–3822. (f) Rodrigues, R. R.; Chance M. Boudreaux, C. M.; Papish, E. T.; Delcamp, J. H. Photocatalytic Reduction of CO_2 to CO and Formate: Do Reaction Conditions or Ruthenium Catalysts Control Product Selectivity? *ACS Appl. Energy Mater.* **2019**, *2*, 37–46.

(6) (a) Ghosh, D.; Takeda, H.; Fabry, D. C.; Tamaki, Y.; Ishitani, O. Supramolecular Photocatalyst with a Rh(III)-Complex Catalyst Unit for CO_2 reduction. *ACS Sustainable Chem. Eng.* **2019**, *7*, 2648–2657. (b) Tamaki, Y.; Ishitani, O. Supramolecular Photocatalysts for the Reduction of CO_2. *ACS Catal.* **2017**, *7*, 53394-3409. (c) Chen, L.; Qin, Y.; Chen, G.; Li, M.; Cai, L.; Qiu, Y.; Fan, H.; Robert, M.; Lau, T.-C. A Molecular Noble Metal-Free System for Efficient Visible Light-Driven Reduction of CO_2 to CO. *Dalton Trans.* **2019**, *48*, 9596–9602. (d) Hong, D.; Kawanishi, T.; Tsukakoshi, Y.; Kotani, H.; Ishizuka, T.; Kojima, T. Efficient Photocatalytic CO_2 Reduction by a Ni(II) Complex Having Pyridine Pendants through Capturing a Mg^{2+} Ion as a Lewis-Acid Cocatalyst. *J. Am. Chem. Soc.* **2019**, *141*, 20309–20317.

(7) (a) Takeda, H.; Koike, K.; Inoue, H.; Ishitani, O. Development of an Efficient Photocatalytic System for CO_2 Reduction Using Rhenium(I) Complexes Based on Mechanistic Studies. *J. Am. Chem. Soc.* **2008**, *130*, 2023–2031. (b) Sampson, M. D.; Froehlich, J. D.; Smieja, J. M.; Benson, E. E.; Sharp, I. D.; Kubiak, C. P. Direct Observation of the Reduction of Carbon Dioxide by Rhenium Bipyridine Catalysts. *Energy Environ. Sci.* **2013**, *6*, 3748–3755. (c) Maurin, A.; Ng, C.-O.; Chen, L.; Lau, T.-C.; Robert, M.; Ko, C.-C. Photochemical and electrochemical catalytic reduction of CO_2 with NHC-containing dicarbonyl rhenium(I) bipyridine complexes. *Dalton Trans.* **2016**, *45*, 14524–14529. (d) Hameed, Y.; Berro, P.; Gabidullin, B.; Richeson, D. An integrated Re(I) photocatalyst/sensitizer that activates the formation of formic acid from reduction of CO_2. *Chem. Commun.* **2019**, *55*, 11041–11044.

(8) (a) Chauvin, J.; Lafolet, F.; Chardon-Noblat, S.; Deronzier, A.; Jakonen, M.; Haukka, M. Towards New Molecular Photocatalysts for CO_2 Reduction: Photo-Induced Electron Transfer versus CO Dissociation within $[Os(NN)(CO)_2Cl_2]$ Complexes. *Chem.–Eur. J.* **2011**, *17*, 4313–4322. (b) Castillo, C. E.; Armstrong, J.; Laurila, E.; Oresmaa, L.; Haukka, M.; Chauvin, J.; Chardon-Noblat, S.; Deronzier, A. *ChemCatChem* **2016**, *8*, 2667–2677.

(9) (a) Sato, S.; Morikawa, T.; Kajino, T.; Ishitani, O. A Highly Efficient Mononuclear Iridium Complex Photocatalyst for CO_2 Reduction under Visible Light. *Angew. Chem., Int. Ed.* **2013**, *125*, 1022–1026. (b) Sato, S. Morikawa, T.; Kajino, T.; Ishitani, O. A Highly Efficient Mononuclear Iridium Complex Photocatalyst for CO_2 Reduction under Visible Light. *Angew. Chem., Int. Ed.* **2013**, *52*, 988 –992. (c) Garg, K.; Matsubara, Y.; Ertem, M. Z.; Lewandowska-Andralojc, A.; Sato, S.; Szalda, D. J.; Muckerman, J. T.; Fujita, E. Striking Differences in Properties of Geometric Isomers of

[Ir(tpy)(ppy)H]$^+$: Experimental and Computational Studies of their Hydricities, Interaction with CO_2, and Photochemistry. *Angew. Chem., Int. Ed.* **2015**, *54*, 14128–14132. (d) Genoni, A.; Chirdon, D. N.; Boniolo, M.; Sartorel, A.; Bernhard, S.; Bonchio, M. Tuning Iridium Photocatalysts and Light Irradiation for Enhanced CO_2 Reduction. *ACS Catal.* **2017**, *7*, 154–160. (e) Sato, S.; Morikawa, T. [Ir(tpy)(bpy)Cl] as a Photocatalyst for CO_2 Reduction under Visible-Light Irradiation. *ChemPhotoChem* **2018**, *2*, 207 – 212.

(10) (a) Lee, S. K.; Kondo, M.; Okamura, M.; Enomoto, T.; Nakamura, G.; Masaoka, S. Function-Integrated Ru Catalyst for Photochemical CO_2 Reduction. *J. Am. Chem. Soc.* **2018**, *140*, 16899–16903. (b) Das, S.; Rodrigues, R. R.; Lamb, R. W.; Qu, F.; Reinheimer, E.; Boudreaux, C. M.; Webster, C. E.; Delcamp, J. H.; Papish, E. T. Highly Active Ruthenium CNC Pincer Photocatalysts for Visible-Light-Driven Carbon Dioxide Reduction. *Inorg. Chem.* **2019**, *58*, 8012–8020.

(11) (a) Rao, H.; Bonin, J.; Robert, M. Non-sensitized Selective Photochemical Reduction of CO_2 to CO under Visible Light with an Iron Molecular Catalyst. *Chem. Commun.* **2017**, *53*, 2830–2833. (b) Bonin, J.; Chaussemier, M.; Robert, M.; Routier, M. Homogeneous Photocatalytic Reduction of CO_2 to CO Using Iron(0) Porphyrin Catalysts: Mechanism and Intrinsic Limitations. *ChemCatChem* **2014**, *6*, 3200–3207. (c) Behar, D.; Dhanasekaran, T.; Neta, P. Cobalt Porphyrin Catalyzed Reduction of CO_2. Radiation Chemical, Photochemical, and Electrochemical Studies. *J. Phys. Chem. A* **1998**, *102*, 2870–2877.

(12) (a) Miura, T.; Held, I. E.; Oishi, S.; Naruto, M.; Saito, S. Catalytic Hydrogenation of Unactivated Amides Enabled by Hydrogenation of Catalyst Precursor. *Tetrahedron Lett.* **2013**, *54*, 2674–2678; (b) Miura, T.; Naruto, M.; Toda, K.; Shimomura, T.; Saito, S. Multifaceted Catalytic Hydrogenation of Amides via Diverse Activation of a Sterically Confined Bipyridine–ruthenium Framework. *Sci. Rep.* **2017**, *7*, 1586. (c) Hashimoto, A.; Yamaguchi, H.; Suzuki, T.; Kashiwabara, K.; Kojima, M.; Takagi, H. Preparation, Crystal Structures, and Spectroscopic and Redox Properties of Nickel(II) Complexes Containing Phosphane–(Amine or Quinoline)-Type Hybrid Ligands and a Nickel(I) Complex Bearing8-(Diphenylphosphanyl)quinoline. *Eur. J. Inorg. Chem.***2010**, 39–47. (d) Nimura, S.; Yoshioka, S.; Naruto, M.; Saito, S., Reaction of H_2 with Mitochondria-Relevant Metabolites Using a Multifunctional Molecular Catalyst. ChemRxiv. Preprint (2020).

(13) (a) Zhu, S.-F.; Zhou, Q.-L. Iridium-Catalyzed Asymmetric Hydrogenation of Unsaturated Carboxylic Acids. *Acc. Chem. Res.* **2017**, *50*, 988–1001. (b) Li, J.-Q.; Liu, J.; Krajangsri, S.; Chumnanvej, N.; Singh, T.; Andersson, P. G. Asymmetric Hydrogenation of Allylic Alcohols Using Ir–N,P–Complexes. *ACS Catal.* **2016**, *6*, 8342–8349.

(14) When CO_2 photoreduction was performed in an anhydrous DMA solution, the reactivity in 24 h irradiation (total TON = 193) is lower than those (total TON = 386) in a mixed DMA/H_2O (v/v = 9:1) solution (Table S1; entry 2 and 3) probably due to stabilization of a transition state by hydrogen bonding interactions with H_2O; Dub, P. A.; Gordon, J. C. Metal–Ligand Bifunctional Catalysis: The "Accepted" Mechanism, the Issue of Concertedness, and the Function of the Ligand in Catalytic Cycles Involving Hydrogen Atoms. *ACS Catal.***2017**, *7*, 6635–6655.

(15) Hatchard, C. G.; Parker, C. A. A New Sensitive Chemical Actinometer. II. Potassium Ferrioxalate as a Standard Chemical Actinometer. *Proc. R. Soc. London, Ser. A* **1956**, *235*, 518–536.

(16) Nakagawa, T.; Okamoto, K.; Hanada, H.; Katoh, R. Probing with Randomly Interleaved Pulse Train Bridges the Gap between Ultrafast Pump-probe and Nanosecond Flash Photolysis. *Opt. Lett.* **2016**, *41*, 1498–1501.

(17) (a) Ballardini, R.; Varani, G.; Indelli, M. T.; Scandola, F. Phosphorescent 8-Quinolinol Metal Chelates. Excited-State Properties and Redox Behavior. *Inorg. Chem.* **1986**, *25*, 3858-3865. (b) Liu, X.-Y.; Zhang, Y.-H.; Fang, W.-H.; Cui, G. Early-Time Excited-State Relaxation Dynamics of Iridium Compounds: Distinct Roles of Electron and Hole Transfer. *J. Phys. Chem. A* **2018**, *122*, 5518–5532.

(18) Kavarnos, G. J. *Fundamentals of Photoinduced Electron Transfer*; Wiley-VCH: New York, 1993.

(19) (a) Marcus, R. A. Chemical and Electrochemical Electron-Transfer Theory. *Annu. Rev. Phys. Chem.* **1964**, *15*, 155–196. (b) Marcus, R. A. Electron Transfer Reactions in Chemistry: Theory and Experiment. *Angew. Chem., Int. Ed. Engl.* **1993**, *32*, 1111–1121.

(20) (a) Tamaki, Y.; Koike, K.; Morimoto, T.; Ishitani, O. Substantial Improvement in the Efficiency and Durability of a Photocatalyst for Carbon Dioxide Reduction Using a Benzoimidazole Derivative as an Electron Donor. *J. Catal.* **2013**, *304*, 22–28. (b) Hasegawa, E.; Takizawa, S.; Seida, T.; Yamaguchi, A.; Yamaguchi, N.; Chiba, N.; Takahashi, T.; Ikeda, H.; Akiyama, K. Photoinduced Electron-Transfer Systems Consisting of Electron-Donating Pyrenes or Anthracenes and Benzimidazolines for Reductive Transformation of Carbonyl Compounds. *Tetrahedron* **2006**, *62*, 6581–6588.

(21) The *g* parameters exhibited that the spin density in the OERS is predominantly located on bipyridine (bpy). However, the large *g* anisotropy cannot be simply described as an $Ir^{III}(bpy^{\bullet-})$ complex suggested by other groups, signifying isomeric form between Ir(II) and Ir(III)($bpy^{\bullet-}$).

(22) (a) Bokarev, S. I.; Hollmann, D.; Pazidis, A.; Neubauer, A.; Radnik, J.; Kühn, O.; Lochbrunner, S.; Junge, H.; Beller, M.; Brückner, A. Spin Density Distribution after Electron Transfer from Triethylamine to an $[Ir(ppy)_2(bpy)]^+$ Photosensitizer during Photocatalytic Water Reduction. *Phys. Chem. Chem. Phys.* **2014**, *16*, 4789–4796. (b) Bruin, B.; Peters, T. P. J.; Thewissen, S.; Blok, A. N. J.; Wilting, J. B. M.; Gelder, R.; Smits, J. M. M.; Gal, A. W. Dioxygen Activation by a Mononuclear Ir^{II}–Ethane Complex. *Angew. Chem. Int. Ed.* **2002**, *41*, 2135–2138. (c) Stinner, C.; Wightman, M. D.; Kelley, S. O.; Hill, M. G.; Barton, J. K. Synthesis and Spectroelectrochemistry of Ir(bpy)(phen)$(phi)^{3+}$, a Tris(heteroleptic) Metallointercalator. *Inorg. Chem.* **2001**, *40*, 5245-5250.

(23) Dragonetti, C.; Falciola, L.; Mussini, P.; Righetto, S.; Roberto, D.; Ugo, R.; Valore, A. The Role of Substituents on Functionalized 1,10-Phenanthroline in Controlling the Emission Properties of Cationic Iridium(III) Complexes of Interest for Electroluminescent Devices. *Inorg. Chem.* **2007**, *46*, 8533-8547.

(24) (a) Suenobu, T.; Guldi, D. M.; Ogo, S.; Fukuzumi, S. Excited-State Deprotonation and H/D Exchange of an Iridium Hydride Complex. *Angew. Chem., Int. Ed.* **2003**, *42*, 5492–5495. (b) Wiedner, E. S.; Chambers, M. B.; Pitman, C. L.; Bullock, R. M.; Alexander J. M. Miller, A. J. M.; Appel, A. M. Thermodynamic Hydricity of Transition Metal Hydrides. *Chem. Rev.* **2016**, *116*, 8655–8692.

(25) Schmeier, T. J.; Dobereiner, G. E.; Crabtree, R. H.; Hazari, N. Secondary Coordination Sphere Interactions Facilitate the Insertion Step in An Iridium(III) CO_2 Reduction Catalyst. *J. Am. Chem. Soc.* **2011**, *133*, 9274–9277.

(26) (a) Oldenhof, S.; van der Vlugt, J. I.; Reek, J. N. H. Hydrogenation of CO_2 to formic acid with $iridium^{III}$(bisMETAMORPhos)(hydride): the role of a dormant *fac*-Ir^{III}(trihydride) and an active *trans*-Ir^{III}(dihydride) species. *Catal. Sci. Technol.* **2016**, *6*, 404–408. (b) Li, H.; Wang, X.; Huang, F.; Lu, G.; Jiang, J.; Wang, Z.-X. Computational Study on the Catalytic Role of Pincer Ruthenium(II)-PNN Complex in Directly Synthesizing Amide from Alcohol and Amine: The Origin of Selectivity of Amide over Ester and Imine. *Organometallics* **2011**, *30*, 5233–5247.

(27) Cyclic voltammograms suggest that CO_2 reacts with OERS of **1** which has an Ir–H bond and there are many literatures to report that CO_2 insertion into M–H bond gives HCOOH; Wang, W.-H.; Himeda, Y.; Muckerman, J. T.; Manbeck, G. F.; Fujita, E. CO_2 Hydrogenation to Formate and Methanol as an Alternative to Photo- and Electrochemical CO_2 Reduction. *Chem. Rev.* **2015**, *115*, 12936–12973.

(28) As long as we know, there are no report that CO was produced after CO_2 insertion into an Ir–H bond. CO should be formed after formation of M–CO_2H complex; Yamazaki, Y.; Takeda, H.; Ishitani, O. Photocatalytic Reduction of CO_2 Using Metal Complexes. *J. Photochem. Photobiol. C* **2015**, *25*, 106–137.

TOC Graph

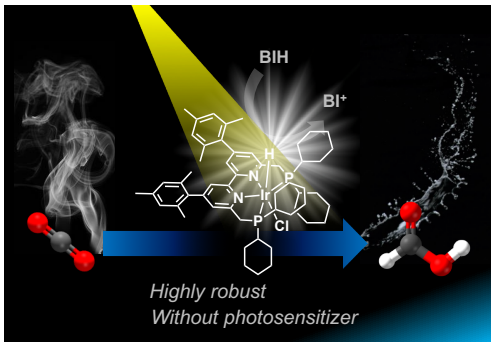

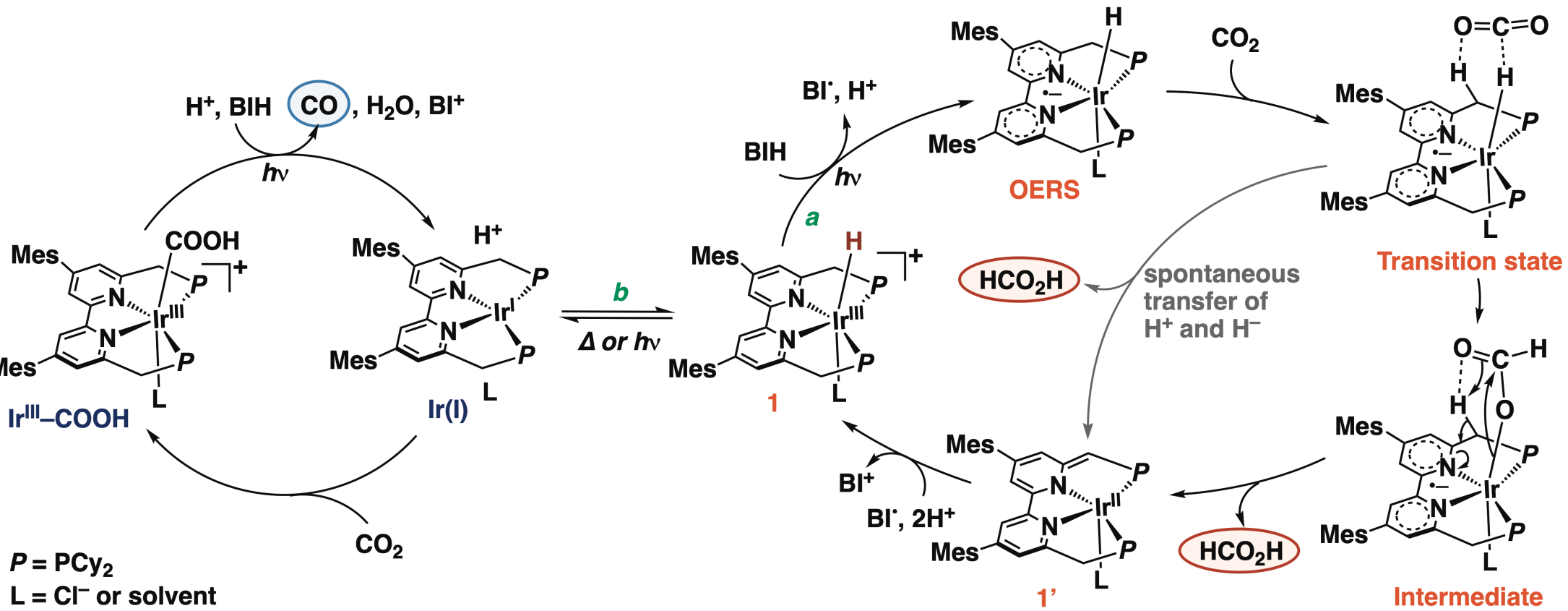
H+, BIH
CO
, H2O, BI+
hν
COOH
Mes
Mes
Ir^III–COOH
H+
Ir(I)
CO2
b
Δ or hν
a
BIH
hν
BI•, H+
H
1
OERS
CO2
Transition state
spontaneous transfer of H+ and H−
HCO2H
Intermediate
HCO2H
BI+
BI•, 2H+
1'
P = PCy2
L = Cl− or solvent

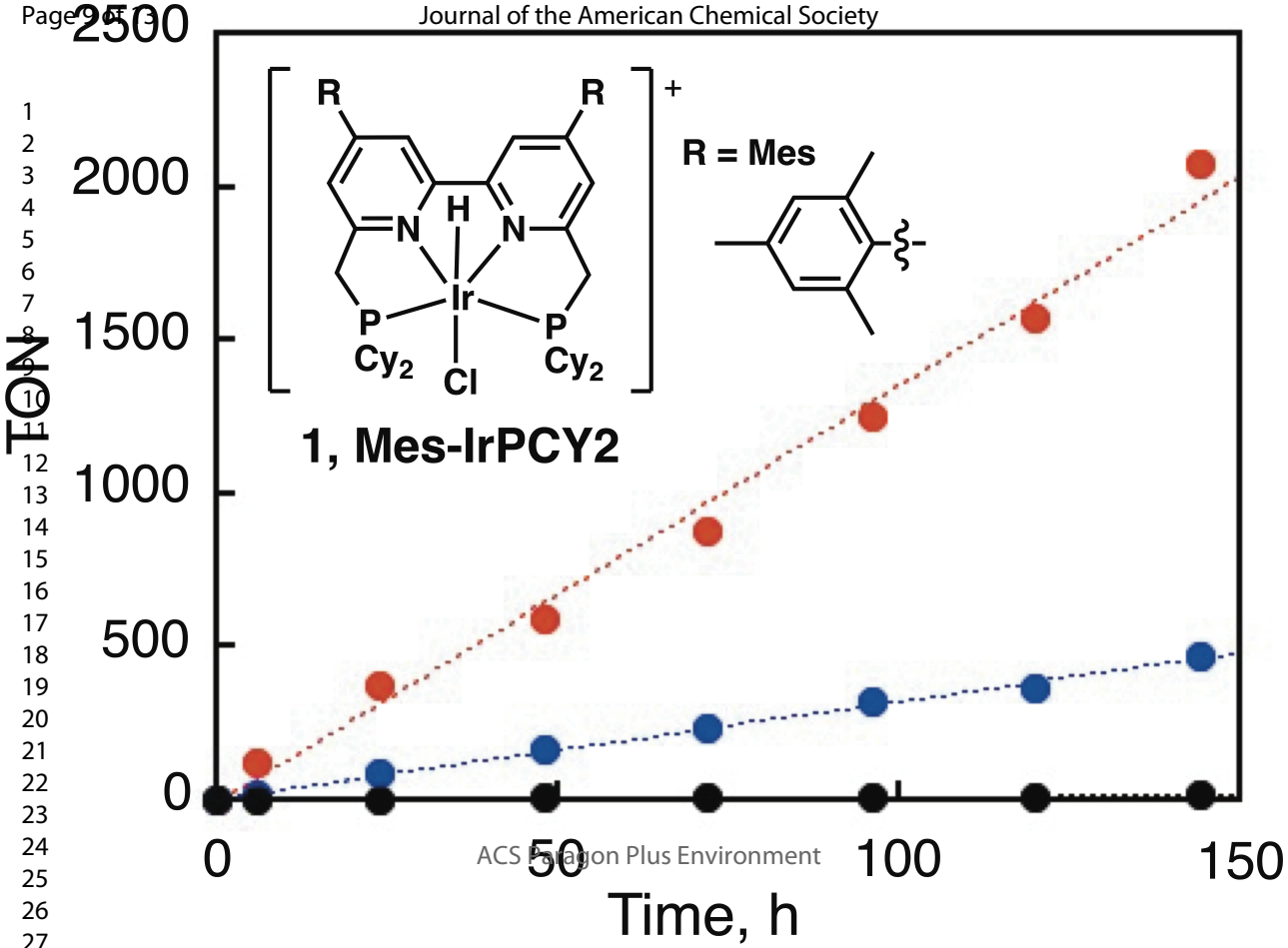
R
R
+
H
N
N
Ir
P
P
Cy2
Cy2
Cl
1, Mes-IrPCY2
R = Mes
TON
2500
2000
1500
1000
500
0
0
50
100
150
Time, h

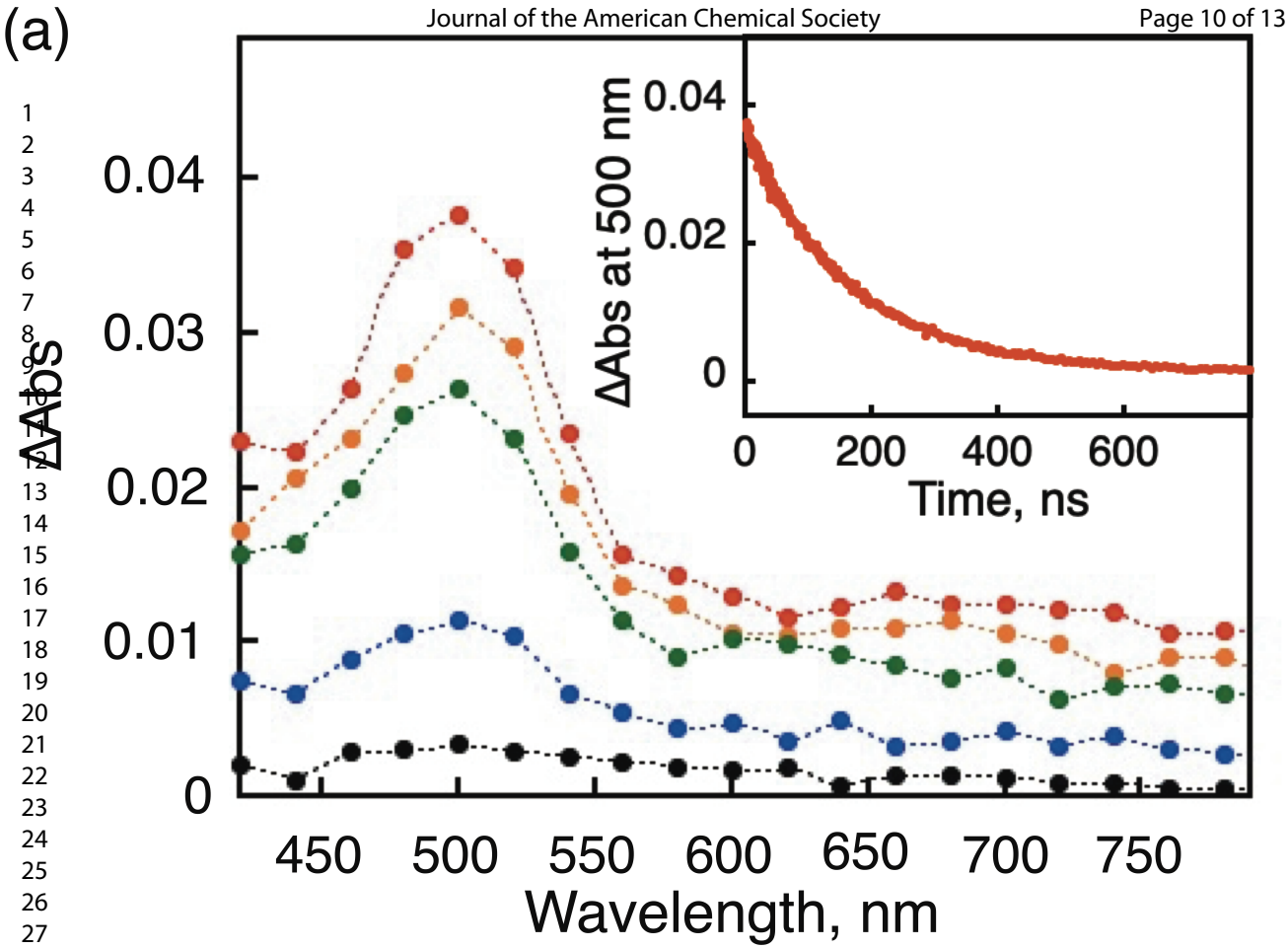
(a)
ΔAbs
0.04
0.03
0.02
0.01
0
450
500
550
600
650
700
750
Wavelength, nm
ΔAbs at 500 nm
0.04
0.02
0
0
200
400
600
Time, ns

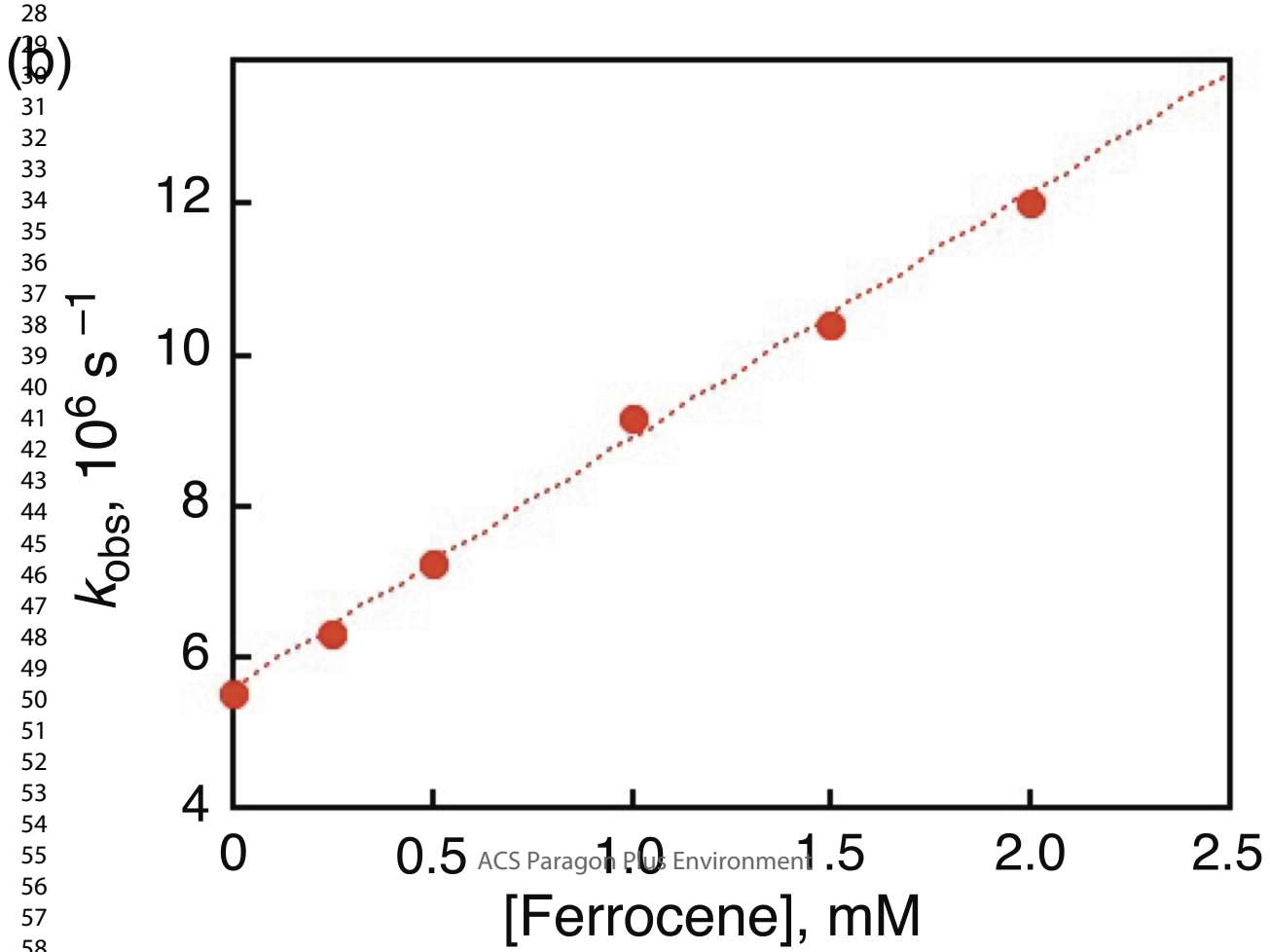
(b)
k_{obs}, 10^6 s^{-1}
12
10
8
6
4
0
0.5
1.0
1.5
2.0
2.5
[Ferrocene], mM

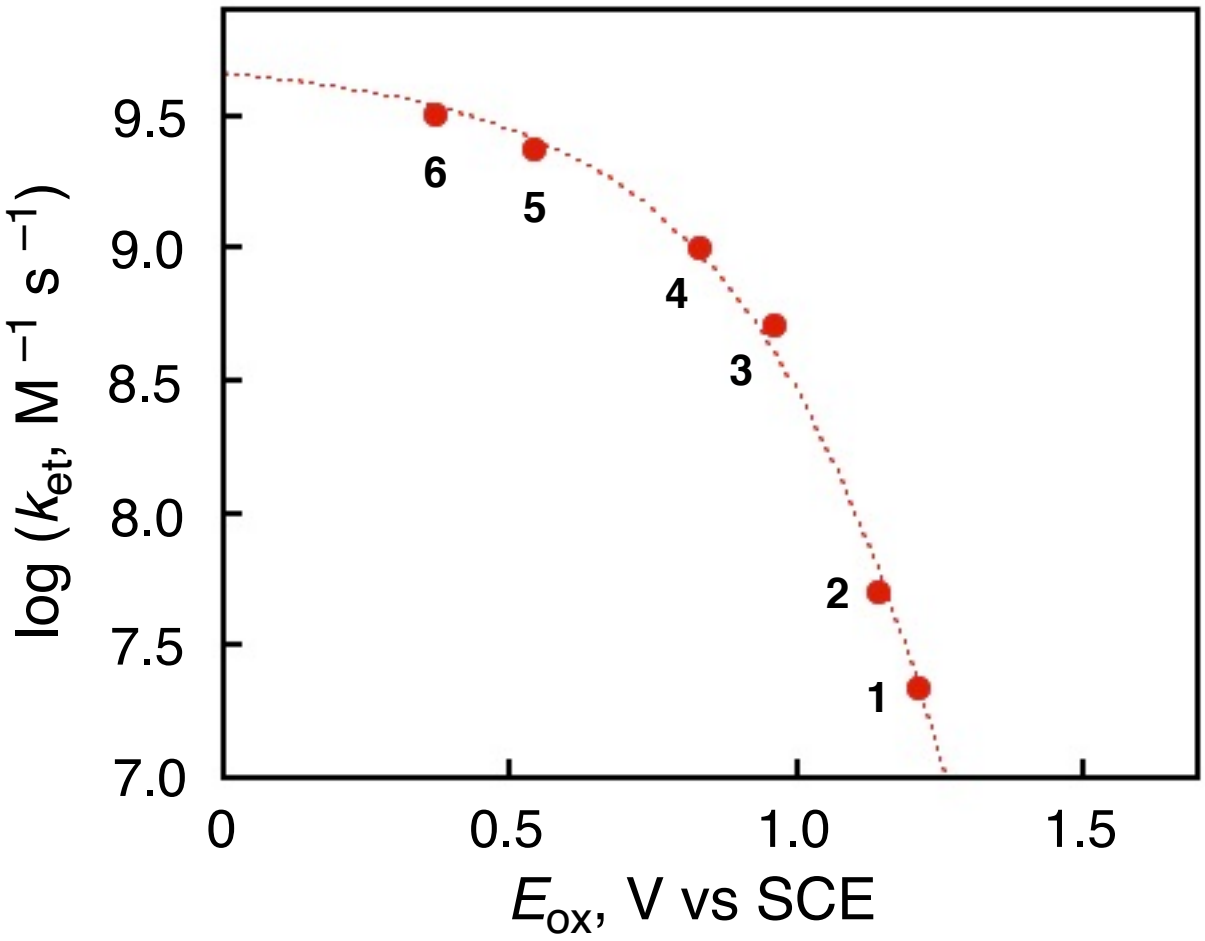
log (k_{et}, M^{-1} s^{-1})
9.5
9.0
8.5
8.0
7.5
7.0
0
0.5
1.0
1.5
E_{ox}, V vs SCE
6
5
4
3
2
1